Electronic Supplementary Material (ESI) for Nanoscale.

Te-S covalent bond induces 1T&2H MoS_2 with improved potassium-ion storage performance

Wei Kang,[1,#] Ruicong Xie, [1,#] Yuchen Wang,[1] Cuihua An,[1,2,] Chao Li[1,]**

[1] Tianjin Key Laboratory of Advanced Functional Porous Materials, Center for Electron Microscopy, Institute for New Energy Materials & Low-Carbon Technologies, School of Materials Science and Engineering, Tianjin University of Technology, Tianjin 300384, China

[2] Key Laboratory of Advanced Energy Materials Chemistry (MOE), College of Chemistry, Nankai University, Tianjin 300071, China

E-mail: ancuihua@tjut.edu.cn; chao_li@tjut.edu.cn

Usually, the electrochemical reaction mechanism can be disclosed based on the following empirical formula:

$$i = av^b \qquad \text{(Equation S1)}$$

Where i is the peak current, v is the scan rate, and a and b are constants. The b value is the slope of the Log(i) and Log(v), which is often used to determine the electrochemical characteristic. If b=0.5, which suggests the electrochemical storage process is full diffusion control. Similarly, if b=1, illustrating that it is the ideal capacitance behavior.

Moreover, the contribution fraction of the above two parts can be quantitative by the following equation:

$$i = k_1 v + k_2 v^{1/2} \qquad \text{(Equation S2)}$$

Where i is the total current contributions that are split by k_1v and $k_2v^{1/2}$, which is a result of the capacitance contribution and the diffusion-controlled insertion procedure, respectively.

Besides, the diffusion coefficients (D) of the 2H MoS_2 and 1T&2H Te-MoS_2 anodes have been calculated from the galvanostatic intermittent titration technique (GITT) plots according to the following equation:

$$D = \frac{4}{\pi\tau}\left(\frac{m_B V_M}{M_B S}\right)^2\left(\frac{\Delta E_s}{\Delta E_\tau}\right)^2 \qquad \text{(Equation S3)}$$

Where τ is the duration of the current pulse, m_B is the mass of the active material in the anodes, M_B is the molar mass of the anode, S is the geometric area of the anode, V_M is the molar volume of the anode, $\triangle E_S$ is the quasi-thermodynamic equilibrium voltage difference before and after the current pulse, $\triangle E_\tau$ is the voltage difference during the current pulse, respectively.

The electronic conductivities of 1T&2H Te-MoS_2 and 2H MoS_2 have been measured by ST-2258A multi-functional digital four-probe meter and SZT-D Semiconductor powder resistivity test plat form. And all of the measurements were conducted at 25 ^oC.

The condition of EIS measurement is as follows. The sinusoidal perturbation amplitude is 0.005 V. The high frequency and low frequency are 10^5 and 10^{-2} Hz, respectively. And the fixed D. C. voltage is 2.0 V.

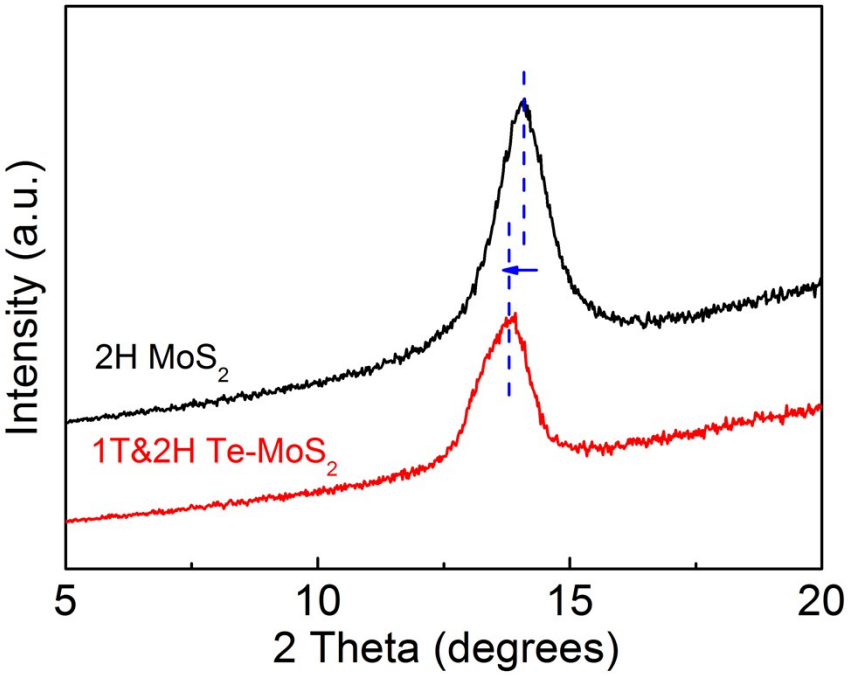

Figure S1 XRD patterns at 5-20° of 2H MoS_2 and 1T&2H Te-MoS_2 materials.

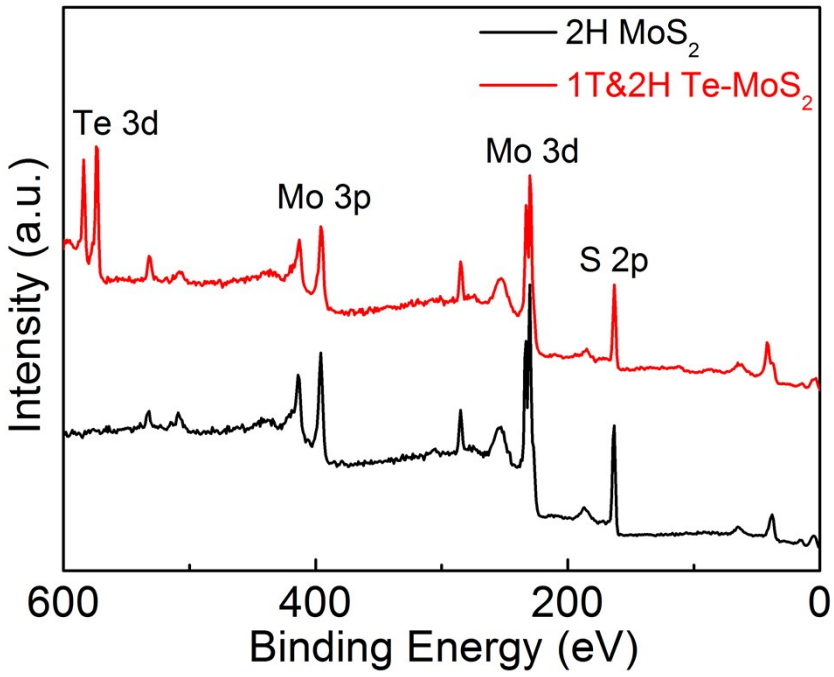

Figure S2 XPS survey spectra of 2H MoS_2 and 1T&2H Te-MoS_2 materials.

Table S1 Relative atomic ratio of elements in 1T&2H Te-MoS_2 materials

	Te at%	Mo at%	S at%
EDS	0.38	33.05	66.57
XPS	0.35	33.42	66.23

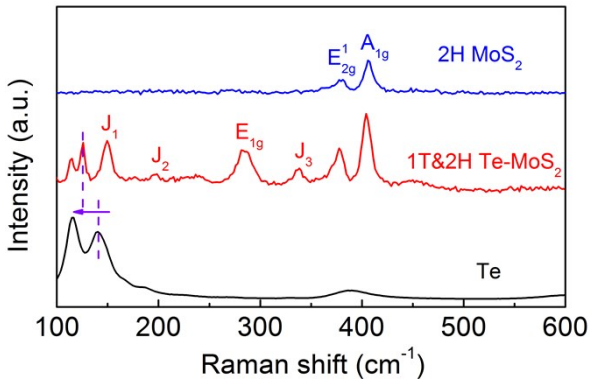

Figure S3 Raman spectra of 2H MoS_2, 1T&2H Te-MoS_2 and the commercial Te powder materials.

And the Raman spectra of 2H MoS_2, 1T&2H Te-MoS_2 and the commercial Te powder have been exhibited in Figure S3. The Raman spectroscopy provides direct evidence of Te doping-induced partial phase transformation from 2H to 1T. 2H MoS_2 exhibits two peaks located at 378.6 and 406.2 cm^{-1}, resulting from the in-plane Mo-S phonon mode (E^1_{2g}), and out-of-plane Mo-S mode (A_{1g}), respectively.[1-3] In contrast, 1T&2H Te-MoS_2 shows new peaks at 149.8, 196.5, 285.2 and 338.0 cm^{-1}, which are significantly related to the J_1, J_2, E_{1g} and J_3 photo modes of 1T-MoS_2, along with the 2H MoS_2 signals (E^1_{2g} and A_{1g}), suggesting the formation of 1T&2H Te-MoS_2.[4-6] Similarly, the commercial Te powder displays three characteristic peaks located at 116.2, 140.4 and 390.3 cm^{-1}, respectively, which is consistent with the previous literatures. For 1T&2H Te-MoS_2, after Te doping into MoS_2, the small peak at 390.3 cm^{-1} disappears, although the vibration peaks around 116.2 cm^{-1} of Te remains, indicating that the Te is not only physical confined in MoS_2, but is also chemically bonded to sulfur of MoS_2, which replaces partially Mo ions in MoS_2.[7-10]

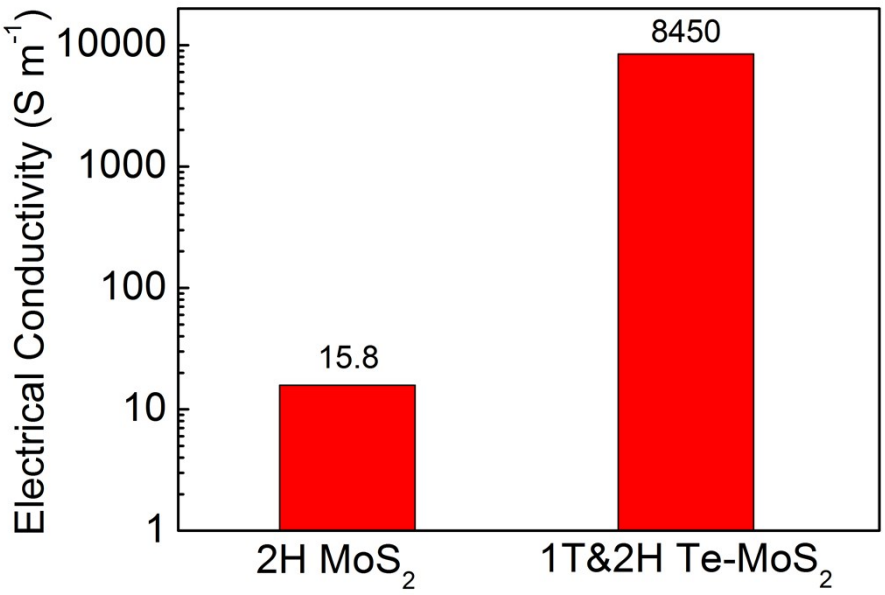

Figure S4 Electrical conductivity of 2H MoS_2 and 1T&2H Te-MoS_2 materials.

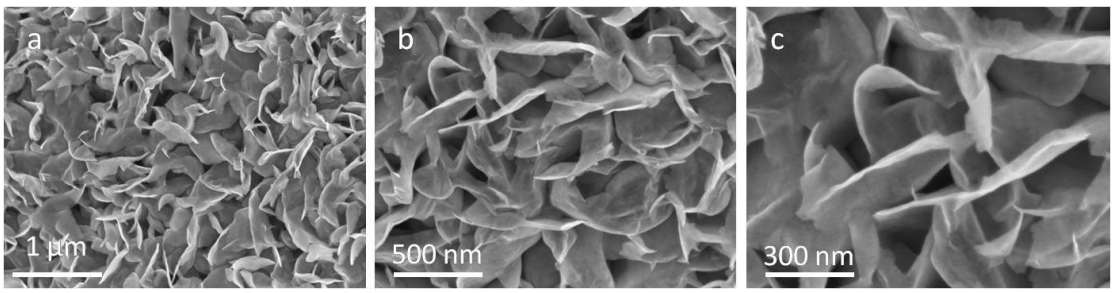

Figure S5 SEM images of 2H MoS_2 materials.

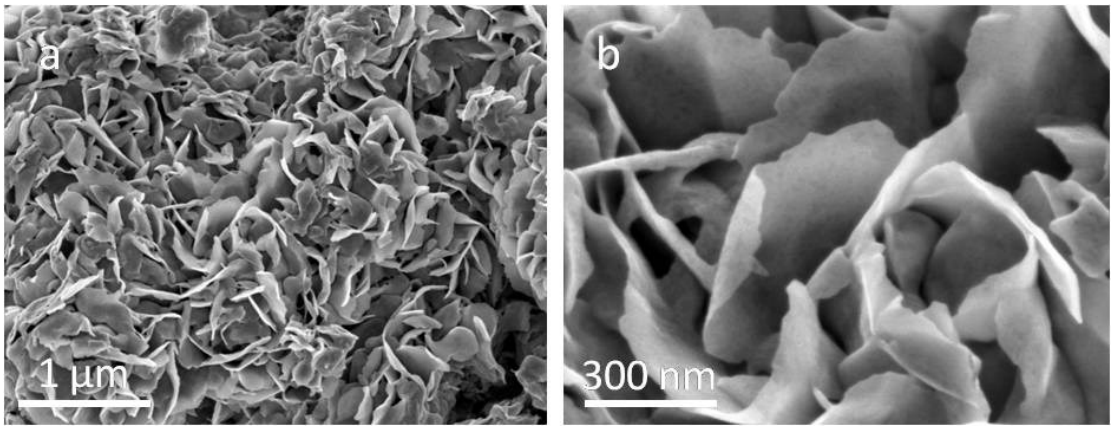

Figure S6 SEM images of 1T&2H Te-MoS_2 materials.

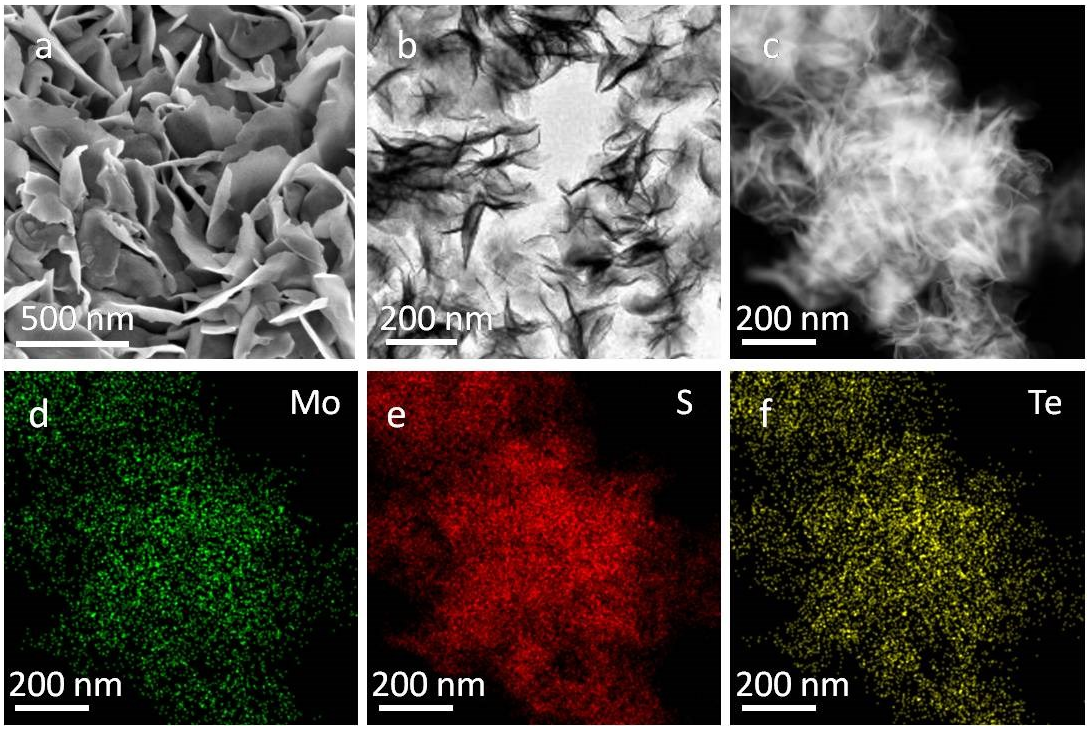

Figure S7 SEM (a), TEM (b) and element mapping (c-f) images of 1T&2H Te-MoS_2 materials.

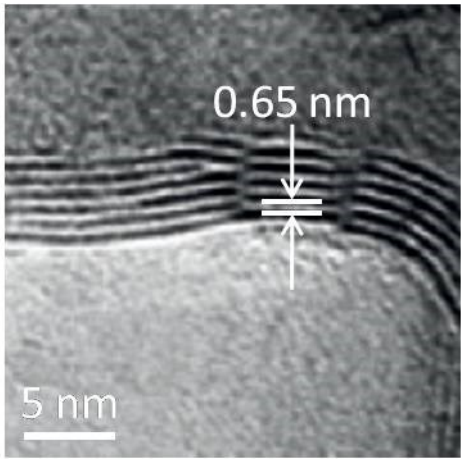

Figure S8 HRTEM images of 1T&2H Te-MoS_2 materials.

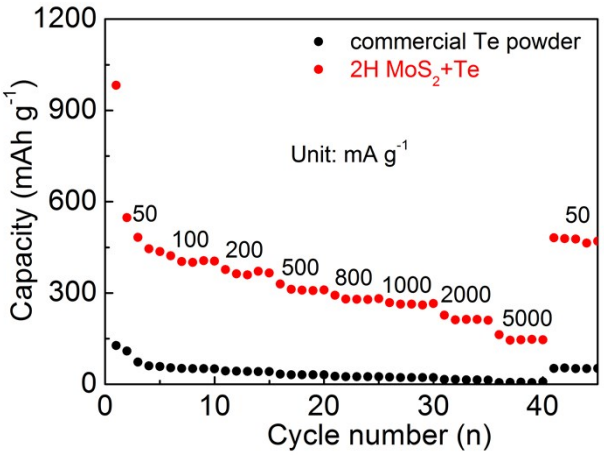

Figure S9 Rate performances of the commercial Te powder and 2H MoS_2+Te electrodes.

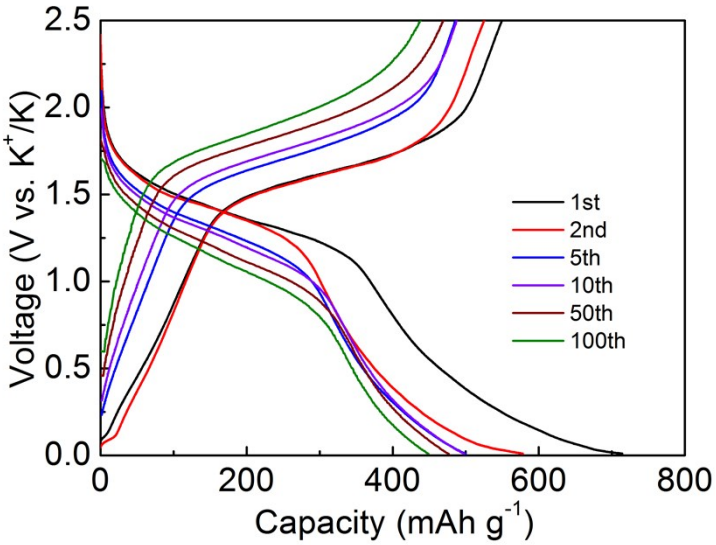

Figure S10 GCD plots of 1T&2H Te-MoS_2 materials at different cycles (100 mA g^{-1} current density).

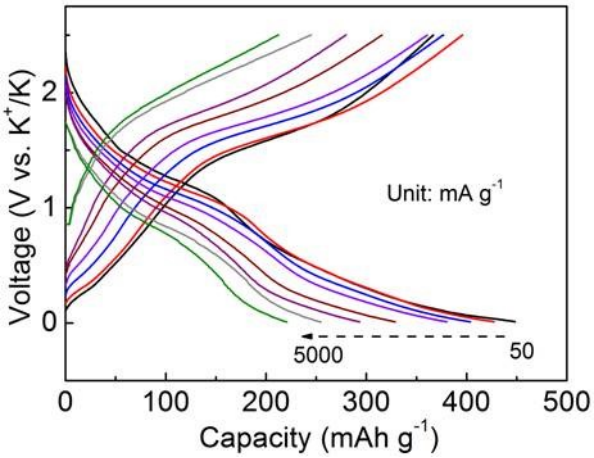

Figure S11 GCD plots of the 2H MoS_2 anode at various current densities.

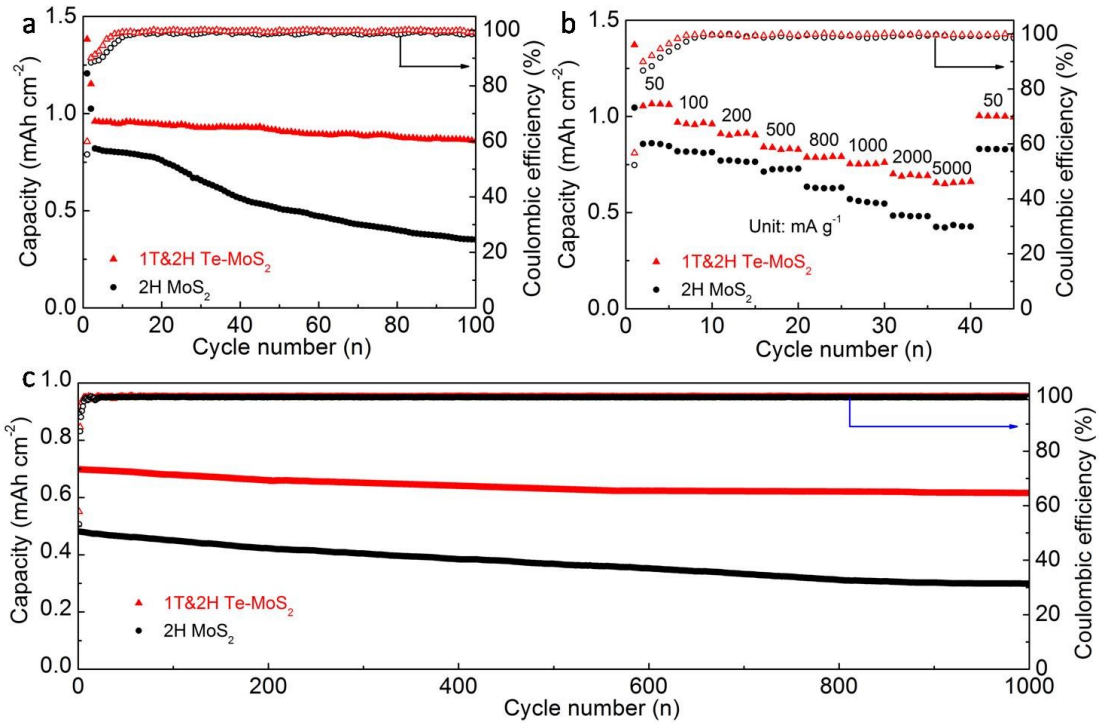

Figure S12 Long cycling stability at 100 mA g^{-1} (a), rate performances (b), cycling performances at 2 A g^{-1} (c) of 2H MoS_2 and 1T&2H Te-MoS_2 electrodes based on the area of the electrode.

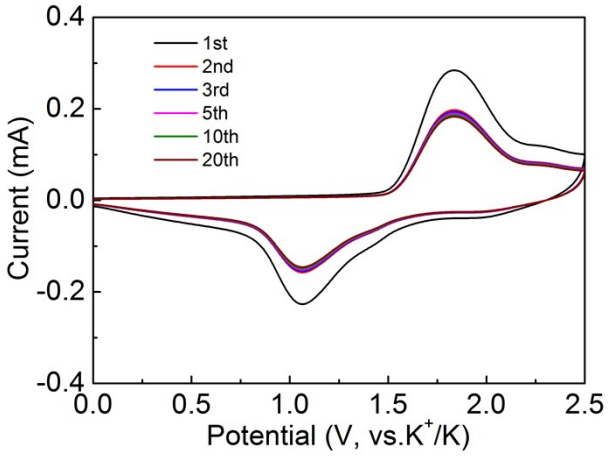

Figure S13 CV curves of 1T&2H Te-MoS_2 materials at different cycles (1 mV s^{-1} scan rate).

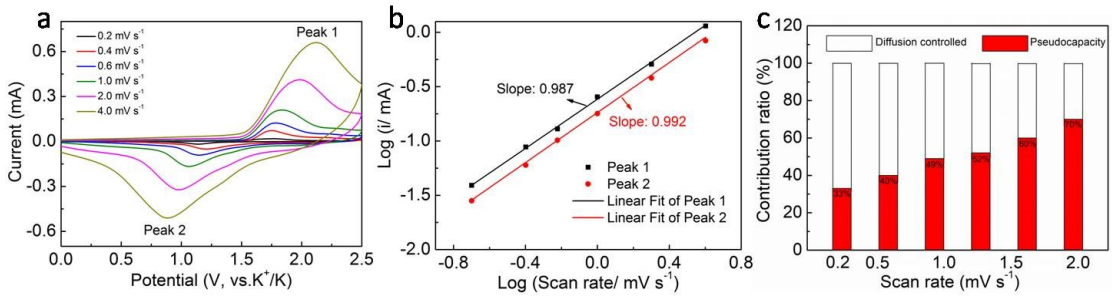

Figure S14 CV curves at different scan rates (a), the Logarithmic relationship between the peak current and the scan rates (b), the percentage contribution of the diffusion controlled and capacitive at various scan rates (c) of 2H MoS_2 anode.

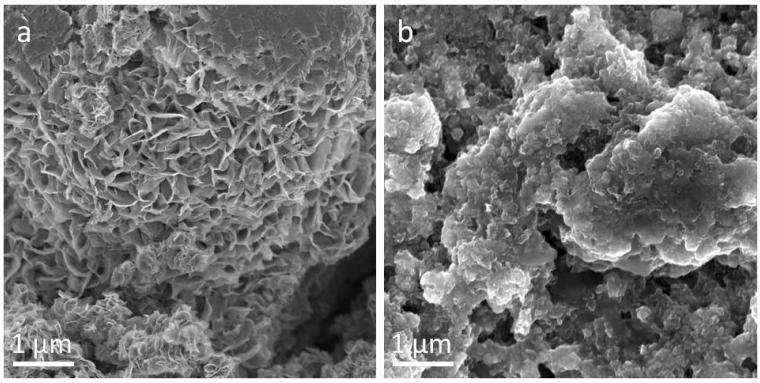

Figure S15 SEM images of 1T&2H Te-MoS_2 (a) and 2H MoS_2 (b) after 50 cycles at 100 mA g^{-1} current density.

References:

[1] F. Güller, A. M. Llois, J. Goniakowski, C. Noguera, Phys. Rev. B, 2015, 91, 075407.

[2] Z. D. Lei, J. Zhan, L. Tang, Y. Zhang, Y. Wang, Adv. Energy Mater., 2018, 1703482.

[3] C. Zhao, C. Yu, B. Qiu, S. Zhou, M. Zhang, H. Huang, B. Wang, J. Zhao, X. Sun, J. Qiu, Adv. Mater., 2018, 30, 1702486.

[4] Z. Chen, K. Leng, X. Zhao, S. Malkhandi, W. Tang, B. Tian, L. Dong, L. Zheng, M. Lin, B. S. Yeo, K. P. Loh, Nat. Commun., 2017, 8, 14548.

[5] S. Wang, D. Zhang, B. Li, C. Zhang, Z. Du, H. Yin, X. Bi, S. Yang, Adv. Energy Mater., 2018, 8, 1801345.

[6] A. J. Hu, C. Z. Shu, C. X. Xu, J. B. Li, R. X. Liang, R. X. Zheng, M. L. Li, Z. Q. Ran, J. P. Long, Chem. Eng. J., 2020, 382, 122854.

[7] Y. Liu, J. Wang, Y. Xu, Y. Zhu, D. Bigio, C. Wang, J. Mater. Chem. A, 2014, 2, 12201.

[8] J. Zhang, Y. X. Yin, Y. G. Guo, ACS Appl. Mater. Interfaces, 2015, 7, 27838.

[9] S. Dong, D. D. Yu, J. Yang, L. Jiang, J. W. Wang, L. W. Cheng, Y. Zhou, H. L. Yue, H. Wang, L. Guo, Adv. Mater., 2020, 32, 1908027.

[10] J. Zhang, Y. X. Yin, Y. G. Guo, ACS Appl. Mater. Interfaces, 2015, 7, 27838.